ELSEVIER

Journal of Alloys and Compounds 240 (1996) 219–228

Journal of ALLOYS AND COMPOUNDS

Improvement of the electrochemical activity of Zr–Ni–Cr Laves phase hydride electrodes by secondary phase precipitation

J.-M. Joubert[a,1], M. Latroche[a], A. Percheron-Guégan[a,*], J. Bouet[b]

[a] *Laboratoire de Chimie Métallurgique et de Spectroscopie des Terres Rares, CNRS, 1 Pl. A. Briand, 92195 Meudon Cedex, France*
[b] *DOE, Alcatel Alsthom Recherche, Route de Nozay, 91460 Marcoussis, France*

Received 9 January 1996

Abstract

Within the framework of research on intermetallic compounds for nickel–hydride batteries, we have studied ternary Zr–Ni–Cr alloys. In that system, we have measured both the hydride thermodynamic properties by solid–gas reaction and the electrochemical capacities for ternary Laves phases and binary Zr–Ni intermetallic compounds. A knowledge of the ternary phase diagram has allowed the synthesis of alloys where these two kinds of phase are in equilibrium, at predetermined rates. Study of the electrochemical capacities of these two-phase alloys has shown that the surface modification induced by the precipitation of Zr–Ni binaries considerably enhances the electrochemical capacity discharged by the Laves phase.

Keywords: Laves phase; Metal hydrides; Nickel–hydride batteries; Secondary phases

1. Introduction

The AB_2 (A = Zr, Ti; B = V, Cr, Mn) compounds have been studied for their ability to serve as negative electrodes in nickel–hydride batteries. For example, Laves phases ZrV_2, $ZrCr_2$ and $ZrMn_2$ can be hydrogenated up to 3.6 H per formula unit (H/f.u.), which represents a capacity of 500 mAh g^{-1}. This capacity is larger than that provided by AB_5 type compounds (370 mAh g^{-1}). However, these hydrides are too stable for application. It has been shown [1,2] that substitutions (Ti on the A sublattice; Ni, Fe, and Co on the B sublattice) reduce the cell volume and allow, without too much of a decrease in capacity, hydrides to be obtained with a plateau pressure within the range 0.1–1 bar, compatible with electrochemical applications. However, contrary to AB_5 type compounds, the electrochemical capacities are often lower than those measured by solid–gas reaction. This phenomenon is related to interfacial reaction with the electrolyte (concentrated potassium hydroxide): passivation or surface corrosion induces difficult activation, low kinetics and even jamming of the electrochemical reactions.

In order to overcome these problems, some surface treatments have been investigated. For example, Züttel et al. [3] have studied the influence of different chemical etchings of the alloy surfaces and found that hydrofluoric acid treatment gave the best results with $Zr(V_{1-x}Ni_x)_2$ electrodes. In contrast, a few authors have pointed out the interest of using polyphasic alloys to improve the electrochemical activity of a major phase. For example, Notten and Hokkeling [4] have studied the catalytic effect of nickel precipitates in AB_5 type compounds. Ovonics alloys [5] are multiphase, each phase absorbing hydrogen and said to have a catalytic activity. However, no systematic study had been made to clearly define the role of each phase. At last, a study made by Gutjahr [6] on the discharge capacity of alloys containing various rates of TiNi and Ti_2Ni phases showed that better results are obtained with mixed phases than with each phase taken independently.

We wanted to measure the influence of secondary phase precipitation on Laves phase electrode discharge capacities. A systematic study of the hydrogenation properties and electrochemical capacities was possible in the ternary system Zr–Ni–Cr. This system

* Corresponding author.
[1] Present address: Laboratoire de Cristallographie, Université de Genève, 24 Quai E. Ansermet, 1211 Genéve 4, Switzerland.

0925-8388/96/$15.00
PII S0925-8388(96)02243-8

was chosen because $ZrCr_2$ has a large hydrogen capacity and nickel is a good candidate for hydride destabilization because of small atomic radius and good corrosion resistance. To control the secondary phase precipitation, the ternary phase diagram was established at 1000°C [7]. We have therefore determined the homogeneity region of the Laves phases in the system and obtained information on the nature and composition of secondary phases in equilibrium with them. This determination has permitted, in a second step, the synthesis of single phase and multiphase alloys with Laves phases of definite composition in equilibrium with a variable amount of secondary phases. Then, the hydrogenation properties were investigated by solid–gas reaction. For single phase alloys, the P–c–T curves were determined at room temperature. For multiphase alloys, full capacity and reversible capacity were measured. Finally, the electrochemically discharged capacities were measured for all alloys studied and for a constant Laves phase composition as a function of the secondary phase content.

2. Experimental procedure

The alloys were synthesized by induction melting of the pure elements (Zr 99.9%, Ni 99.9%, Cr 99.99%) into a water cooled copper crucible under argon atmosphere. Every alloy was remelted five times and inverted between each melting to ensure homogeneity. Then it was wrapped in tantalum foil and annealed in a secondary evacuated silica tube at 1000°C for 30 days to ensure equilibrium. The silica tube was then quenched into cold water.

A sample was taken from the alloy and polished for optical and electronic metallographic examination and electron microprobe analysis. An X-ray powder diffractogram was obtained with an automated Phillips PW1752 diffractometer (Cu Kα). It was analyzed with the full pattern fitting program FULLPROF [8] using the Rietveld refinement method. These three methods gave us the number, nature, composition and lattice parameters of the different phases in equilibrium. Moreover, a quantitative phase analysis was conducted using three different techniques. In the first, the quantity of each phase was obtained by a calculation involving the nominal composition and the composition of each phase determined by microprobe analysis. Secondly, the same measurement was obtained by quantitative metallography. Backscattered electron images from a scanning electron microscope were digitalized. The phase ratio was then evaluated by measurement of the different surfaces occupied by each phase. The third method was derived from the Rietveld analysis of the diffractograms. The quantity of each phase was evaluated through the measurement of the integrated intensities corresponding to each phase. The method was previously calibrated using prepared mixings of pure $ZrCr_2$ and Zr_7Ni_{10} phases.

For hydrogenation experiments, samples were mechanically crushed into powder (less than 63 μm) in a glove box under argon atmosphere and introduced into a container so that any exposure to air was avoided. Measurements were made at room temperature with a conventional volumetric method. Two values of hydrogenation capacity were obtained under 10 bar hydrogen pressure: (i) the initial capacity, the capacity absorbed at the first cycle, and (ii) the reversible capacity, the constant capacity obtained during further cycles after outgassing the hydride under constant conditions (15 h, 80°C, primary vacuum). The P–c–T curves were measured with a standard incremental method.

Electrodes were prepared by mixing the alloy (powder crushed under argon atmosphere (less than 36 μm)) (25%) with nickel powder (70%) and PTFE solution (5%) and cold pressing on a nickel grid. Open cells were built by associating these electrodes with $NiOOH/Ni(OH)_2$ positive electrodes. The electrolyte used was KOH (8.7 N). After a partial charge for 1 h under a constant current of 80 mA g^{-1}, the electrodes were exposed to an alkaline etching by heating the accumulator in a drying oven for 3 h at 70°C. The discharge capacities were obtained under constant current conditions with a cut-off potential of 0.9 V. The values of the capacities given at 20 mA g^{-1} were in fact the sum of the capacities discharged successively at 80, 40 and 20 mA g^{-1} after relaxation.

3. Metallurgical synthesis and characterization

3.1. Determination of the phase diagram

The phase diagram of the Zr–Ni–Cr system at 1000°C was determined in the $ZrCr_2$–ZrNi–Ni–Cr region and will be published elsewhere [7]. We describe here the results obtained for the alloys located on the stoichiometric AB_2 line of the phase diagram. These alloys, of nominal composition $Zr(Cr_{1-x}Ni_x)_2$, are identified for simplification with their value of x (e.g. 0.4 for $Zr(Cr_{0.6}Ni_{0.4})_2$). The results of their characterization are given in Table 1.

$ZrCr_2$ (alloy 0.0) was observed with C15 structure in agreement with the phase diagram data at 1000°C [9]. This structure is retained for low nickel substitution. For higher Ni concentrations it is transformed into the C14 structure, the high temperature form of $ZrCr_2$ stabilized by the substitution. A two-phase system, containing C14 and C15 phases, is observed in sample 0.2. The mixing of these two phases is confirmed by

Table 1
Metallurgical characterization of the alloys studied

Name	Nominal composition (at.%)			Phases	Rate (wt.%)	Composition (at.%)			Cell parameters and volume (Å and Å^3 per AB_2 unit)
	Zr	Ni	Cr			Zr	Ni	Cr	
0.0	33.3	0	66.6	C15	100	32.8(6)	—	67.2(6)	$a = 7.211(1)$ $V = 46.87$
0.2	33.3	13.3	33.3	C15		32(1)	10(1)	58(2)	$a = 7.176(2)$ $V = 46.20$
				C14		33.1(5)	16(1)	51(1)	$a = 5.058(2)$ $c = 8.287(4)$ $V = 45.90$
0.4−	32.9	26.6	40.5	C14	96	32.4(6)	27(1)	41(2)	$a = 5.029(1)$ $c = 8.232(1)$ $V = 45.08$
				ZrNi	1				*
				Cr	3				*
0.4	33.3	26.6	40.0	C14	96	32.1(3)	26(1)	41(2)	$a = 5.029(1)$ $c = 8.236(1)$ $V = 45.11$
				ZrNi	2	48.8(2)	49.6(3)	1.6(3)	*
				Cr	2				*
0.4+	36	32	32	C14	82	32.9(4)	29.7(3)	37.4(5)	$a = 5.023(1)$ $c = 8.223(2)$ $V = 44.92$
				ZrNi	18	49.7(4)	48.6(4)	1.7(5)	$a = 3.263(4)$ $b = 9.937(20)$ $c = 4.112(7)$
0.4++	38.5	35.5	26	C14	66	32.7(4)	30(1)	36(1)	$a = 5.024(1)$ $c = 8.225(1)$ $V = 44.94$
				ZrNi	34	49.5(2)	49.9(2)	0.6(3)	$a = 3.260(3)$ $b = 9.957(10)$ $c = 4.110(4)$
0.5−	32.7	31.7	35.6	C14	94	31.7(3)	32(1)	36(1)	$a = 5.015(1)$ $c = 8.205(1)$ $V = 44.69$
				Zr_9Ni_{11}	3	43.6(2)	54.7(4)	1.7(5)	*
				Cr	3				*
0.5	33.3	33.3	33.3	C14	94	32.3(1)	33.6(5)	34.1(5)	$a = 5.013(1)$ $c = 8.203(1)$ $V = 44.63$
				Zr_9Ni_{11}	5	44(1)	54.7(8)	1.6(5)	*
				Cr	1				*
0.5+	34.5	37	28.5	C14	85	32.4(1)	33.9(8)	33.6(7)	$a = 5.009(1)$ $c = 8.193(1)$ $V = 44.51$
				Zr_9Ni_{11}	11	43.6(5)	55.4(3)	1.0(2)	$a = 9.878(3)$
				Zr_7Ni_{10}	4	41.0(1)	57.7(2)	1.3(2)	*
0.5+ +	37	41.5	21.5	C14	63	32.4(3)	35.2(5)	32.5(3)	$a = 5.009(1)$ $c = 8.196(1)$ $V = 44.53$
				Zr_9Ni_{11}	37	43.4(2)	55.5(3)	1.1(3)	*
0.575	33.3	38.3	28.3	C14		32.1(1)	35.6(5)	32.2(5)	$a = 5.008(1)$ $c = 8.191(2)$ $V = 44.48$
				C15		31.9(3)	38.0(4)	30.1(5)	$a = 7.074(1)$ $V = 44.25$
				Zr_7Ni_{10}		40.6(1)	58.0(2)	1.5(1)	$a = 9.219(30)$ $b = 9.191(20)$ $c = 12.344(20)$
0.6−	32.3	39.1	28.6	C15	86	31.7(5)	38.9(8)	29(1)	$a = 7.068(1)$ $V = 44.13$

Table 1 *continued*

Name	Nominal composition (at.%)			Phases	Rate (wt.%)	Composition (at.%)			Cell parameters and volume (Å and Å^3 per AB_2 unit)
	Zr	Ni	Cr			Zr	Ni	Cr	
				C14	8				$a = 5.008(2)$ $c = 8.196(5)$ $V = 44.51$
				Zr_7Ni_{10}	6	40.6(5)	57.1(8)	2(1)	$a = 9.219(10)$ $b = 9.171(10)$ $c = 12.379(10)$
0.6	33.3	40.0	26.6	C15	91	32.3(3)	39.1(7)	29(1)	$a = 7.066(1)$ $V = 44.11$
				Zr_7Ni_{10}	9	41.3(3)	57.2(3)	1.5(2)	$a = 9.220(25)$ $b = 9.200(25)$ $c = 12.346(18)$
0.6_{1175}	see text			C15	100	31.6(1)	37.8(3)	30.6(3)	$a = 7.070(1)$ $V = 44.18$
0.6+	33.5	42.5	24	C15	85	31.9(4)	40.9(3)	27.1(3)	$a = 7.060(1)$ $V = 43.99$
				Zr_7Ni_{10}	15	40.7(3)	57.9(2)	1.4(2)	$a = 9.206(12)$ $b = 9.183(12)$ $c = 12.347(10)$
0.6++	35.5	46.25	18.25	C15	64	32.1(1)	41.3(3)	26.7(3)	$a = 7.061(1)$ $V = 44.00$
				Zr_7Ni_{10}	36	41.0(2)	57.6(2)	1.4(2)	$a = 9.204(8)$ $b = 9.183(9)$ $c = 12.352(6)$
0.7	33.3	46.7	20.0	C15	81	32.3(1)	44.6(5)	23.0(4)	$a = 7.040(1)$ $V = 43.62$
				Zr_7Ni_{10}	19	41.4(3)	57.0(6)	1.6(7)	$a = 9.210(7)$ $b = 9.170(7)$ $c = 12.344(7)$
0.8	33.3	53.3	13.3	C15	76	31.3(2)	52.0(2)	16.7(2)	$a = 7.004(1)$ $V = 42.95$
				Zr_7Ni_{10}	24	40.7(3)	58.2(3)	1.1(1)	$a = 9.201(8)$ $b = 9.171(9)$ $c = 12.346(7)$
0.95	33.3	3.3	63.3	C15		28.9(1)	66.4(1)	4.7(1)	$a = 6.940(1)$ $V = 41.78$
				Zr_7Ni_{10}		39.5(2)	59.9(2)	0.5(1)	$a = 9.188(12)$ $b = 9.169(12)$ $c = 12.353(6)$
1.0	33.3	66.6	—	Zr_7Ni_{10}		41.0(2)	59.0(2)	—	$a = 9.180(12)$ $b = 9.196(13)$ $c = 12.363(12)$
				Zr_8Ni_{21}		28.0(1)	71.9(1)	—	$a = 6.513(6)$ $\alpha = 75.3(1)°$ $b = 8.050(6)$ $\beta = 67.8(1)°$ $c = 8.542(8)$ $\gamma = 75.2(1)°$

* Diffracted lines are visible but the phase is present in too small a quantity for measuring reliable lattice parameters.

the Rietveld refinement of the diffractogram and by the two different nickel contents found by microprobe analysis (10 at.% Ni and 16 at.% Ni). The C14 phase extends up to 36 at.% Ni, then a new change is observed in sample 0.575 where the two Laves phases C14 (36 at.% Ni) and C15 (38 at.% Ni) are in equilibrium.

The replacement of chromium by nickel involves a constant diminution of the cell volume of the Laves phase consistent with the smaller atomic radius of nickel (1.24 instead of 1.30 Å). This cell volume per AB_2 unit is calculated by dividing the cell volume by the cell multiplicity (i.e. 4 for C14 structure, 8 for C15 structure). The substitution is also accompanied by a progressive diminution of zirconium stoichiometry down to 28.9 at.% in sample 0.95. This phenomenon causes the precipitation of secondary phases when stoichiometric AB_2 samples are synthesized. These phases are very low chromium substituted Zr–Ni binary compounds: ZrNi for sample 0.4 and Zr_9Ni_{11} for sample 0.5 (Laves phases of the C14 type) and Zr_7Ni_{10} for samples 0.6 to 0.95 (Laves phases of the C15 type). In this last sample, we noticed that the Laves phase exists with C15 structure up to very low

chromium content ($Zr_{28.9}Ni_{66.4}Cr_{4.7}$) but disappears in an alloy of composition $ZrNi_2$ where we observed the equilibrium between Zr_7Ni_{10} and Zr_8Ni_{21} phases in agreement with the binary diagram Zr–Ni [10]. These results can be schematized as in Fig. 1.

3.2. Synthesis of alloys with predetermined phase abundance

Owing to the expected thermodynamic properties of their hydrides, the Laves phases with nickel content between 25 and 40 at.% are of most interest. We have determined by microprobe analysis the positions of three tie-lines in the phase diagram, observed in the samples 0.4, 0.5 and 0.6. In these alloys the Laves phases with 26 at.% Ni (C14), 34 at.% Ni (C14) and 39 at.% Ni (C15) are in equilibrium with ZrNi, Zr_9Ni_{11} and Zr_7Ni_{10}. By shifting along the tie-lines these results allow the calculation of the nominal compositions of new alloys in which the composition and structure of the Laves phase is preserved and the amount of secondary phase can be adjusted to about 20% (alloys called 0.4+, 0.5+ and 0.6+) and 40% (0.4++, 0.5++ and 0.6++). Moreover, in order to obtain single phases, three alloys (0.4−, 0.5− and 0.6−) were synthesized, using as nominal compositions those of the Laves phases measured by microprobe analysis in samples 0.4, 0.5 and 0.6. The nominal compositions of all alloys studied are reported in Fig. 1. All these new alloys were synthesized and equilibrated under the same conditions as the previous ones.

The results of the metallurgical characterizations of all these alloys are shown in Table 1. In each group of alloys (0.4, 0.5 and 0.6 groups) we notice that the nature of the phases in equilibrium (structure of the Laves phase and nature of the secondary phase) is preserved along the tie-lines. Two exceptions are found for the alloys 0.5+ and 0.6−, for which small quantities of Zr_7Ni_{10} and C14 phases are observed. These effects are both due to the proximity and relative narrowness of the two- and three-phase regions in that part of the phase diagram [7]. In the first case (0.5+), because of similar effects, the quantity of Zr_7Ni_{10} (4%) has been added to that of Zr_9Ni_{11} (11%) and it has therefore been assumed that this Laves phase was in equilibrium with 15% of Zr_9Ni_{11}. The compositions and cell volumes of the Laves phases observed in each group of alloys are sufficiently close to state that their physical properties (i.e. hydrogenation and electrochemical properties) will be preserved within the given group.

In the alloys 0.4−, 0.5− and 0.6−, synthesized in order to obtain single Laves phases, we observed generally Cr and/or binary Zr–Ni phases in addition to the Laves phases. This is due to the very narrow homogeneity domain of the Laves phases as a function of the zirconium stoichiometry, to its non-congruent crystallization in that region of the diagram which causes a remaining non-equilibrium even after annealing, and finally to the uncertainty of microprobe analysis composition. Because of its negligible hydriding properties, the Cr phase weight when present has been removed from the total weight of alloys in the calculations.

Because of a particularly high content of Zr_7Ni_{10} as secondary phase in sample 0.6− (6%), a new attempt was made in order to obtain a single Laves phase compound. The alloy, identified as 0.6_{1175}, was obtained by a particular synthesis method. This technique consists of liquid–solid segregation of an alloy of composition 0.6 annealed for 15 days at 1175°C in a region of the phase diagram where the Laves phase is in equilibrium with the liquid phase. After quenching, the pure Laves phase of expected composition can be isolated from the crystallized part corresponding to the liquid.

The results obtained for quantitative phase analysis are generally in good agreement between each of the

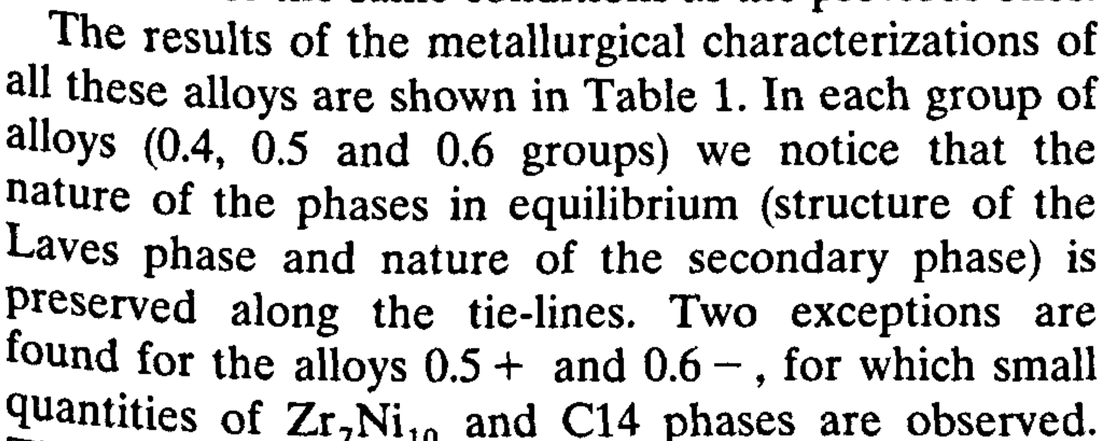

Fig. 1. Schematic presentation of the Zr–Ni–Cr phase diagram at 1000°C for zirconium concentrations between 20 and 50 at.%. The zirconium rich border of the Laves phase homogeneity range, the different synthesized compositions and the tie-lines used for the synthesis of two-phase alloys of predetermined composition are shown. For a more accurate presentation see Ref. [7].

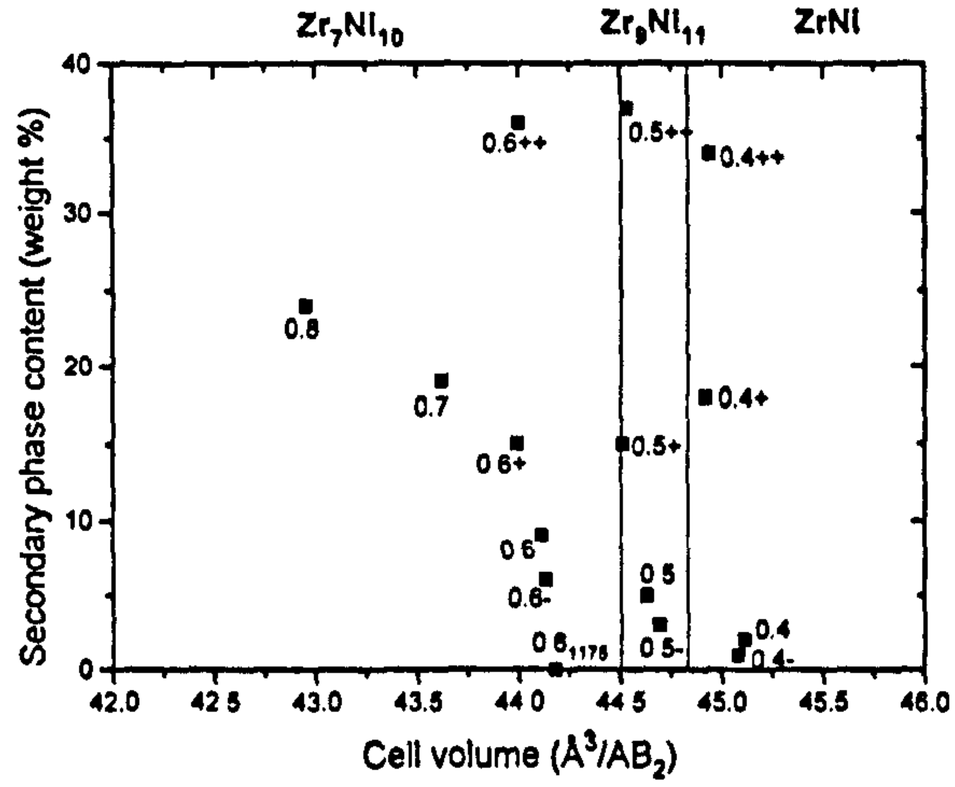

Fig. 2. Amount and nature of secondary phases in equilibrium as a function of the cell volume of the Laves phase per AB_2 formula unit.

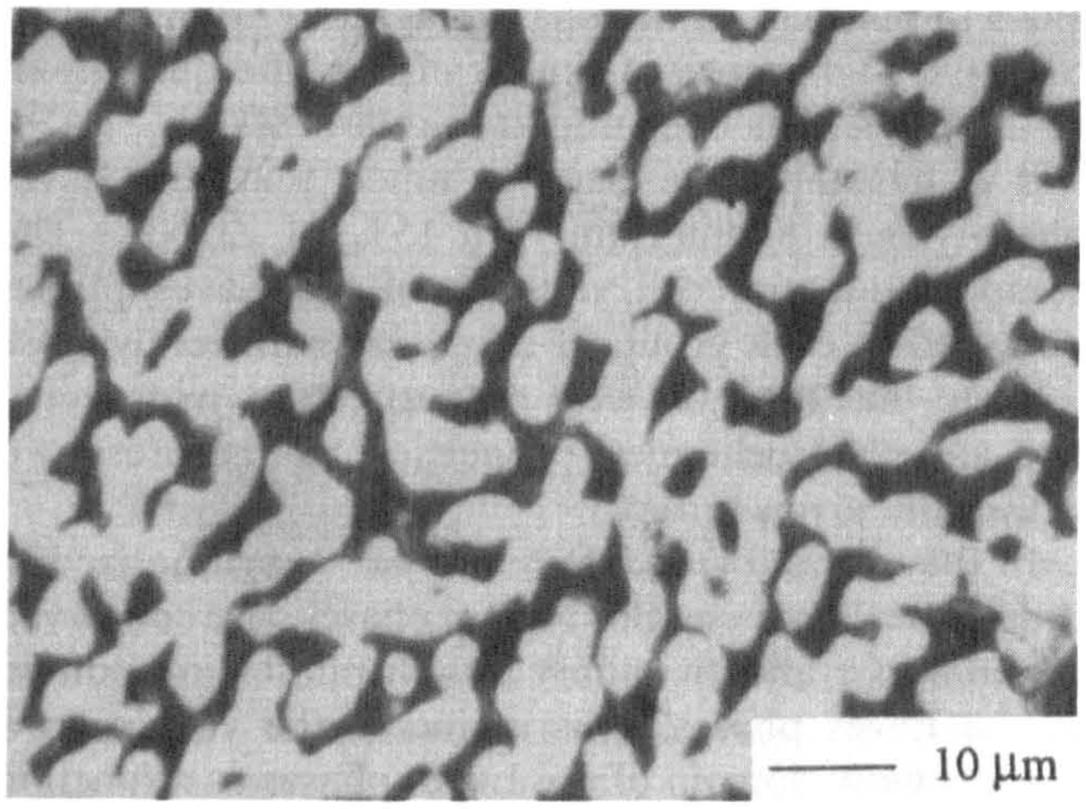

Fig. 3. Optical micrograph of alloy 0.6 + + : C15 (white) and Zr_7Ni_{10} (black) phases.

three methods described in detail in Section 2 (standard deviations about 2%). The values given in Table 1 are the mean of the three results.

Fig. 2 summarizes the metallurgical characterizations for the alloys involved in hydrogenation measurements, giving for each alloy, as a function of the cell volume of the Laves phase (per AB_2 unit), the nature and amount of the secondary phases. The cell volume has been chosen to represent the characteristics of the Laves phase because it is very sensitive to phase composition changes and is related to the thermodynamic properties of its hydrides. An example of metallographic microstructure is shown in Fig. 3 for alloy 0.6 + + . It can be seen that the two phases (C15 and Zr_7Ni_{10}) are so finely precipitated that they will still be in contact in each electrochemical grain (less than 36 μm).

4. Hydrogenation measurements

4.1. Capacity measurements

The results obtained for the different alloys (initial and reversible capacities) are listed in Table 2. Because of multiphase alloys, they are expressed in millimoles of hydrogen atoms per gram of alloy (mmolH g^{-1}). The values given for Zr–Ni binaries have been published elsewhere [11], except the values for ZrNi (this work). These results can be plotted for each group of alloys as a function of the amount of secondary phase (Figs. 4(a) to 4(c)). The reversible capacities are systematically less than the initial capacities. This means that the alloy has absorbed its full capacity during the first cycle and that the desorption conditions (15 h, 80°C, dynamic primary vacuum) are insufficient to outgas all the hydrogen content.

The variation in capacity as a function of the amount of secondary phase is linear. This proportionality with the phase abundance implies that each phase absorbs and desorbs hydrogen as if present alone. The straight lines can be extrapolated to single Laves phases. The capacities obtained, now expressed in hydrogens per formula unit, are listed in Table 3 and plotted in Fig. 5. The initial capacity is firstly constant as a function of nickel substitution up to 40 at.% Ni, and then decreases. In contrast, the reversible capacity as defined in Section 2, reaches a maximum. This fact can be explained if one considers the competition between two effects: the diminution of the full capacity of hydrides and the increase in their equilibrium pressure leading to a better reversibility.

Table 2
Hydrogen capacities of the different alloys studied (25 °C, 10 bar)

Alloy	Initial capacity (mmolH g^{-1})	Reversible capacity (mmolH g^{-1})
0.4−	17.4	15.1
0.4	17.2	not measured
0.4+	17.3	12.7
0.4++	17.6	11
ZrNi	17.3	3.5
0.5−	16.9	16.0
0.5	16.7	16.0
0.5+	15.9	14.9
0.5++	15.2	12.9
Zr_9Ni_{11}	12.7	6.8
0.6−	16	15
0.6	15.8	15
0.6+	14.8	13.4
0.6++	14.5	12.5
Zr_7Ni_{10}	14	10.7
0.7	11.4	10.7
0.8	6	5.8

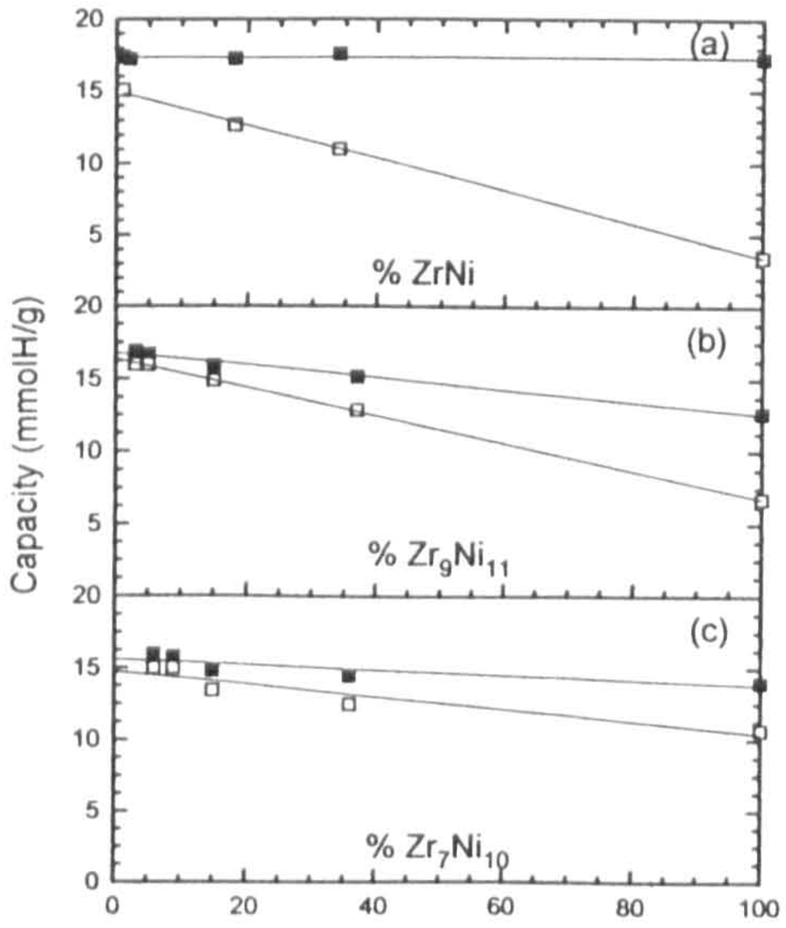

Fig. 4. Initial (■) and reversible (□) hydrogen capacities (25°C, 10 bar) as a function of secondary phase content for the alloys: (a) 0.4 − , 0.4, 0.4 + , 0.4 + + and ZrNi; (b) 0.5 − , 0.5, 0.5 + , 0.5 + + and Zr_9Ni_{11}; (c) 0.6 − , 0.6, 0.6 + , 0.6 + + and Zr_7Ni_{10}.

4.2. P–c–T measurements

P–c–T measurements were performed at 25°C on the alloys 0.5, 0.6, 0.7 and 0.8. In each case, a correction was applied to remove the effect of the secondary phases when present. This correction was possible owing to the knowledge of the P–c–T curves for those alloys determined previously [11]. The isotherms (Fig. 6) consist of a reduced α branch, a plateau pressure corresponding to α–β transition, and finally a wide β branch (e.g. half capacity is absorbed in the β phase for alloy 0.6). As a function of nickel concentration, we observe increasing destabilization of the hydrides. We note also the reduction of the plateau pressure width, which nearly disappears for alloy 0.8.

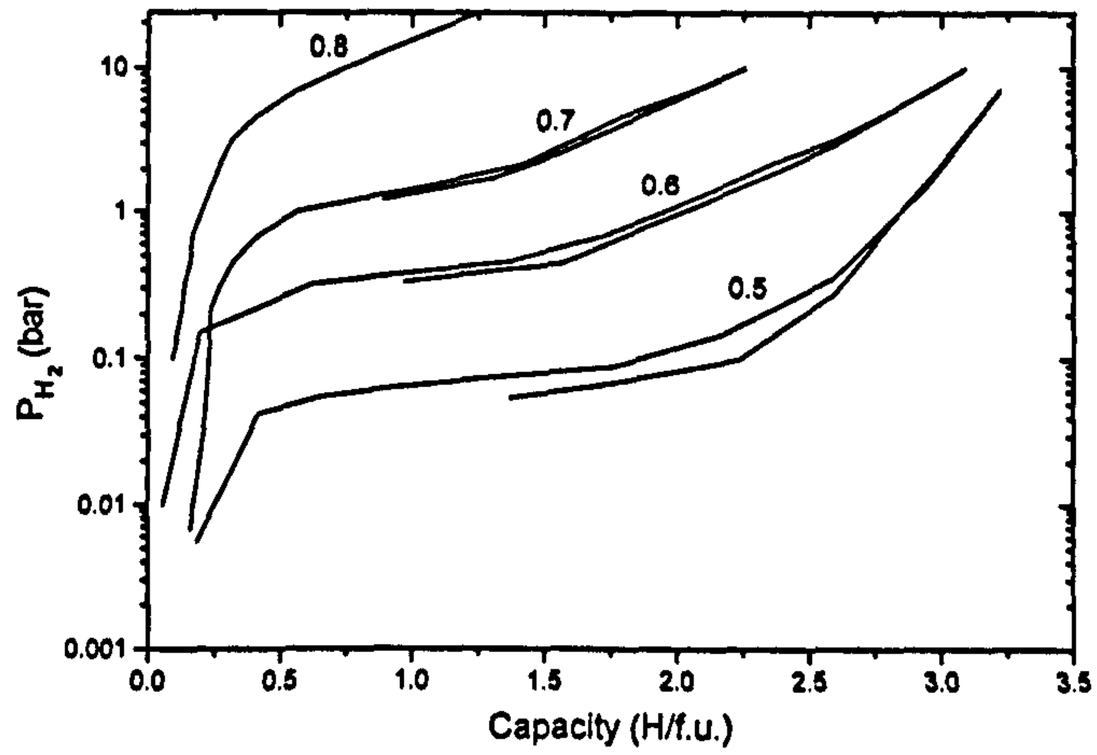

Fig. 6. P–c–T isotherms (25°C) for alloys 0.5, 0.6, 0.7 and 0.8 corrected with secondary phase content.

4.3. Conclusions

The hydriding properties of the major part of the Zr–Ni binary compounds have been determined previously [11]. In this work we have examined, as a function of nickel concentration, the hydrogenation properties of the ternary Laves phases in the system Zr–Ni–Cr. No difference was observed between the hydrides of C14 and C15 phases, neither concerning the capacity nor the stability, except those related to a different composition. Nickel substitution for chromium up to 40 at.% Ni reduces the capacity but not drastically. Simultaneously the plateau pressure increases. It is plotted in Fig. 7 as a function of the cell volume of the intermetallic compound and we can observe that its logarithmic variation is linear, as observed for AB_5 [12] and AB_2 [2] compounds. It is possible to obtain, in this ternary system of hydrides, Laves phases with a plateau pressure in the range 0.1–1 bar, suited for electrochemical application. This is observed for all the Laves phases with a nickel content around 40 at.% (i.e. a cell volume around 44.1 Å^3 per AB_2 unit). It is also observed in the alloys 0.6_{1175}, 0.6−, 0.6, 0.6+ and 0.6++, for which the reversible capacity, expressed in electrochemical units, is superior to 400 mAh g^{-1}. Finally, all the hydrogenation properties of multiphase alloys are a simple combination of the properties of each phase taken independently.

Table 3
Extrapolated hydrogen capacities of Laves phases as a function of nickel content (25 °C, 10 bar)

x	Average nickel rate (at.%)	Initial capacity (mmolH g^{-1} (H/f.u.))	Reversible capacity (mmolH g^{-1} (H/f.u.))
0.0	0	18.0 (3.51)	5.80 (1.13)
0.4	28	17.4 (3.49)	15.0 (3.01)
0.5	33	16.7 (3.37)	16.2 (3.27)
0.6	40	15.6 (3.17)	14.8 (3.01)
0.7	45	10.9 (2.23)	10.7 (2.19)
0.8	52	3.6 (0.74)	3.5 (0.72)

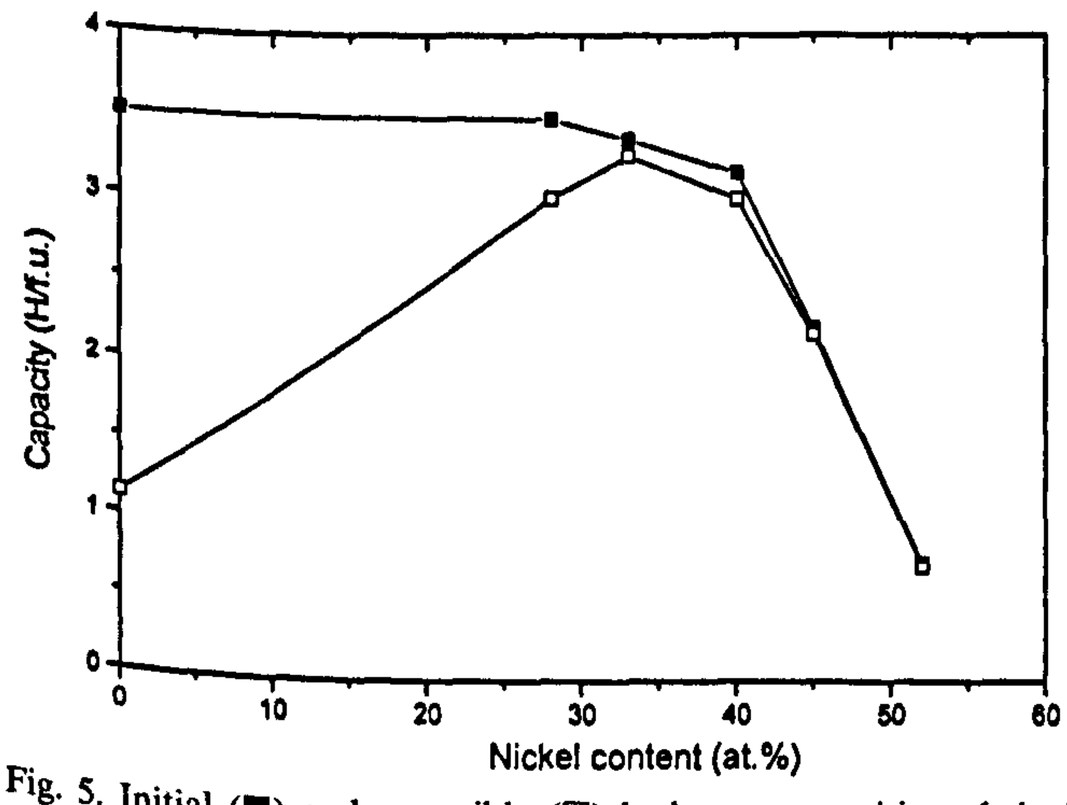

Fig. 5. Initial (■) and reversible (□) hydrogen capacities of single Laves phases (25°C, 10 bar) as a function of nickel concentration.

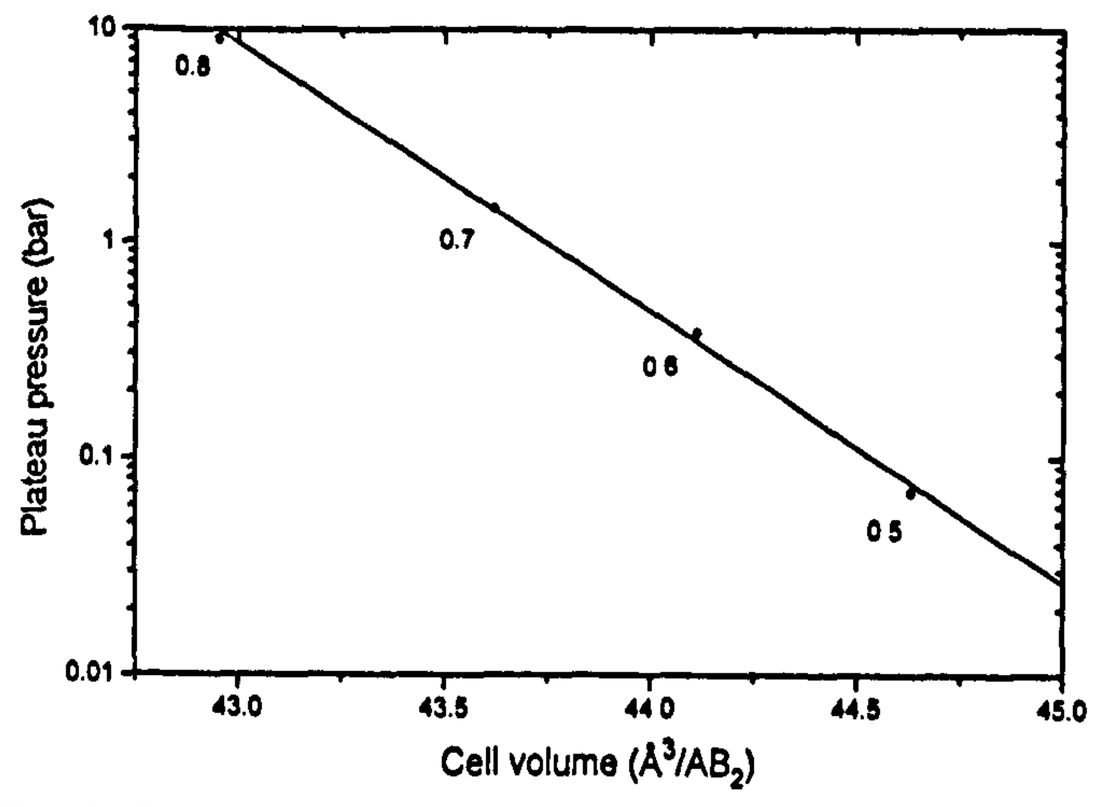

Fig. 7. Equilibrium pressure of Laves phases in the Zr–Ni–Cr system as a function of the cell volume of the intermetallic compound.

5. Electrochemical capacities

5.1. Electrochemical capacities of Zr–Ni binary compounds

The values of the electrochemical capacities of five intermetallic compounds of the Zr–Ni system (ZrNi, Zr_9Ni_{11}, Zr_7Ni_{10}, Zr_8Ni_{21} and Zr_2Ni_7) are presented in Table 4. The capacities are low (less than 100 mAh g^{-1}) except for Zr_8Ni_{21} and Zr_2Ni_7, the two compounds forming the less stable hydrides; they represent 75% of the initial capacity. It seems necessary to correlate these values to the thermodynamic properties of the hydrides determined in Ref. [11]. In Table 4 we compare the discharge capacities with the hydrogen capacities after desorption in solid–gas reactions between 5 and 0.01 bar. The same or better values are obtained for electrochemical capacities, even for Zr_9Ni_{11} for which the 25°C isotherm can be evaluated from the measured values at 100 and 200°C [11].

We can conclude that the poor values of electrochemical capacities obtained for these compounds are explained by the thermodynamic properties of the hydrides. Despite large hydrogen uptake, the low capacities of ZrNi, Zr_9Ni_{11} and Zr_7Ni_{10} are explained by the great stability and low reversibility at room temperature of the corresponding hydrides. The low electrochemical capacities of the hydrides of Zr_8Ni_{21} and Zr_2Ni_7, that have lower stabilities, are simply linked to small solid–gas absorption capacities. For these compounds of the Zr–Ni system, neither activation problems nor cycling capacity decay was observed. This indicates a good surface activity and corrosion resistance.

5.2. Electrochemical capacities of single Laves phases

Experiments were carried out on the Laves phases obtained with a minimum amount of secondary phase. The alloys selected were 0.4 – (1% ZrNi, 3% Cr), 0.5 – (3% Zr_9Ni_{11}, 3% Cr) and 0.6_{1175} (single phase). The capacities (at 20 mA g^{-1} current) are stable from the fourth cycle and are 48 mAh g^{-1} for 0.4 –, 29 mAh g^{-1} for 0.5 – and 25 mAh g^{-1} for 0.6_{1175}. These results are extremely poor compared with the values calculated from the reversible capacities measured by solid–gas reaction (400, 430 and 400 mAh g^{-1} respectively). For alloy 0.6_{1175}, a trial was made to charge the electrode in a sealed cell equipped with a pressure gauge. This reveals that the low capacity is linked to hydrogen gas evolution which starts from the beginning of the charge. It seems that a surface passivation in electrolytic medium inhibits the transfer of hydrogen from electrolyte to bulk material. To check this point, we have changed the surface treatment employed (hot KOH etching) to that proposed by Züttel et al. [3], which seems to give better results with $Zr(V_{1-x}Ni_x)_2$ electrodes. It involves dilute hydrofluoric acid (1%, 5 mn) that is supposed to dissolve the oxides or hydroxides responsible for surface passivation. This treatment was applied to alloy 0.6_{1175}. The electrode charges and discharges in the first cycle a capacity of 215 mAh g^{-1}. However, the discharge capacity decreases rapidly with cycling, as is shown in Fig. 8, recovering finally the values obtained for the non-treated electrode.

The discharge capacities of single Laves phases are very low. These values are not explained by inappropriate thermodynamic properties of the hydrides because it has been shown that either reversible capaci-

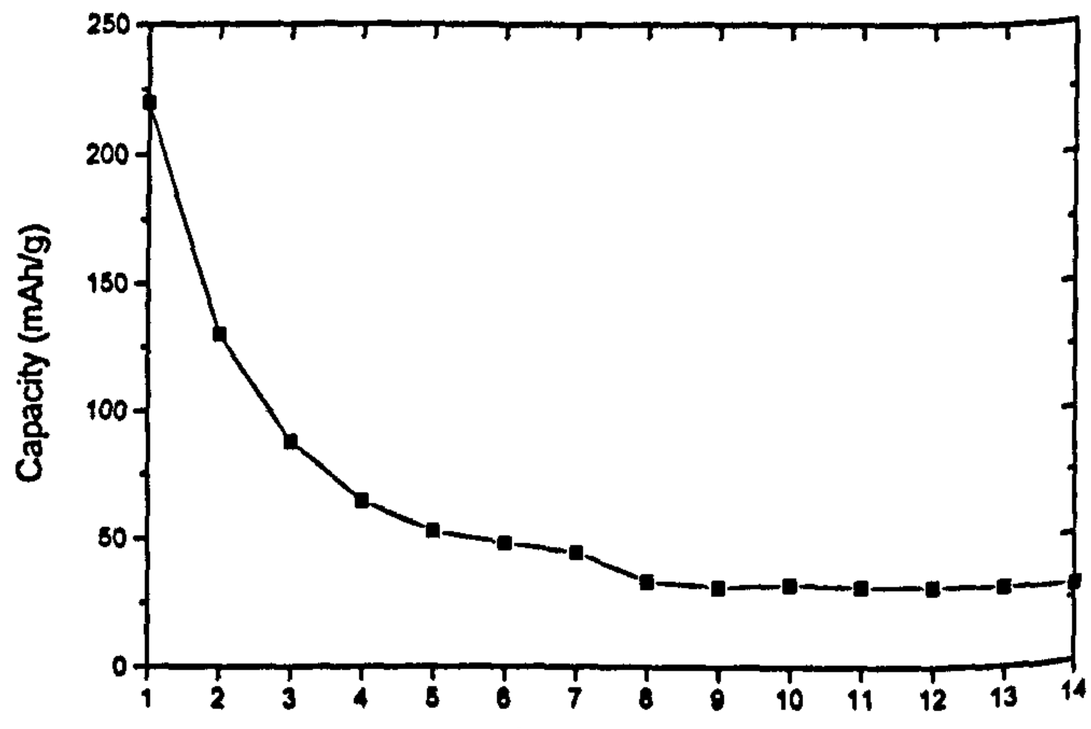

Fig. 8. Discharge capacity (20 mA g^{-1} current) of single phase 0.6_{1175} alloy as a function of cycle number.

Table 4
Comparison between solid–gas and electrochemical capacities for five binary Zr–Ni compounds

Phase	Absorption capacity in solid–gas reaction (25 °C, 10 bar) (mAh g^{-1})	Electrochemically discharged capacity (80 + 40 + 20 mA g^{-1}) (mAh g^{-1})	Desorbed capacity in solid–gas reaction in the range 5–0.01 bar (mAh g^{-1})
ZrNi	460	30	25
Zr_9Ni_{11}	340	95	—
Zr_7Ni_{10}	370	50	40
Zr_8Ni_{21}	120	90	95
Zr_2Ni_7	100	75	50

ties or stabilities were compatible with electrochemical application. They are explained by the absence of electrochemical charge related to surface passivation due to the action of electrolyte on the material. The barrier can be partially removed by hydrofluoric acid attack but forms again rapidly in alkaline solution. These results show the necessity of modifying the surface properties of grains to improve the electrode behaviour. This modification can be obtained by secondary phase precipitation at controlled rate.

5.3. Electrochemical capacities of two-phase alloys

The capacities of each alloy of the three different families were measured under the same conditions (etching 70°C, KOH, 3 h; charge 40 mA g^{-1}; discharge 80 + 40 + 20 mA g^{-1}). The behaviours are comparable: activation during three to five cycles, stable values during ten cycles at least. The values reported in Table 5 are the mean values obtained in the reproducible capacity cycling region. In Figs. 9(a) to 9(c) the total discharged capacities are plotted as a function of the secondary phase rate. We have also plotted the capacity discharged by the Laves phase, calculated considering that the secondary phase has a constant capacity equal to that measured independently and under the same conditions as previously, with the formula

$$C_L = \frac{C_M - x_S C_S}{(1 - x_S)}$$

where C_L is the capacity discharged by the Laves phase, C_M is the total measured discharge capacity, C_S is the capacity of the secondary phase, and x_S is the secondary phase rate.

In each case, i.e. for each type of secondary phase, we observe a spectacular increase of the global discharge capacity, which reaches a maximum at around 20% secondary phase. It decreases with increasing amount of these low capacity phases. In contrast, the real discharge capacity of the Laves phase tends to reach a limit of 120 mAh g^{-1} for alloys in the 0.4 series, 160 mAh g^{-1} for 0.5 and 330 mAh g^{-1} for 0.6.

Table 5
Electrochemical discharge capacities at 80 and 20 mA g^{-1} current

Alloy	Capacity at 80 mA g^{-1} current (mAh g^{-1} (% of total capacity))	Capacity at 20 mA g^{-1} current (mAh g^{-1})
0.4−	11 (23%)	48
0.4	12 (26%)	46
0.4+	35 (34%)	101
0.4++	25 (29%)	86
0.5−	10 (34%)	29
0.5	24 (25%)	96
0.5+	48 (29%)	163
0.5++	65 (50%)	130
0.6_{1175}	15 (60%)	25
0.6−	80 (43%)	186
0.6	110 (48%)	227
0.6+	214 (81%)	263
0.6++	176 (78%)	227

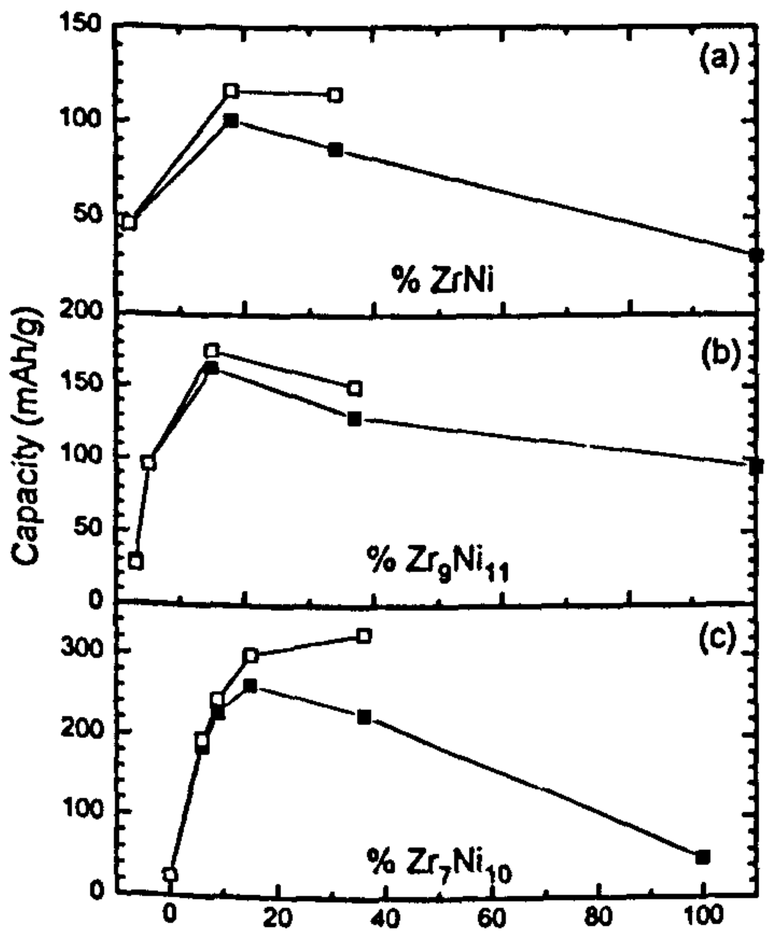

Fig. 9. Discharge capacities (total capacity (■) and discharge capacity of the Laves phase (□)) as a function of secondary phase content for the alloys: (a) 0.4 − , 0.4, 0.4 + , 0.4 + + and ZrNi; (b) 0.5 − , 0.5, 0.5 + , 0.5 + + and Zr_9Ni_{11}; (c) 0.6_{1175}, 0.6 − , 0.6, 0.6 + , 0.6 + + and Zr_7Ni_{10}.

5.4. Discussion

We consider now the results obtained with the alloys of the 0.6 group. These alloys contain various amounts of two phases with strongly different properties.

–The Laves phase (C15, with about 40 at.% Ni) has a reversible hydrogen capacity measured in solid–gas reaction of 400 mAh g^{-1}, 90% of which is absorbed between 0.1 and 10 bar. This pressure range is compatible with the electrochemical reversibility region. However, discharge capacities are low because hydrogen transferring from the electrolyte into the bulk material is inhibited by a jamming at the interface caused by a passivation layer.

–The Zr_7Ni_{10} phase has a high hydrogen capacity in solid–gas reaction (370 mAh g^{-1}) but a small capacity when studied in the electrochemical reversibility pressure range (40 mAh g^{-1}) (Table 4). The electrochemical capacity (50 mAh g^{-1}) is in agreement with this second value. This means a correct electrochemical process and an absence of interfacial problems.

In the grains involved in electrochemical reactions, two phases are finely mixed (as compared with the grain size (see Fig. 3)): one with interesting bulk properties but a blocking surface, the other with a surface allowing electrochemical mechanisms but inadequate thermodynamic properties. For these different reasons the two phases exhibit very low discharge

capacities when separate. The considerable enhancement of the discharge capacity in the mixed alloy can be explained by the increase in Laves phase capacity, for which a deeper discharge is thermodynamically possible. This enhancement is explained by the modification of surface properties of the grains, i.e. by the appearance at this surface of the secondary precipitated phase. If the Laves phase takes advantage of the presence inside the grain of a new surface between the secondary phase and the electrolyte, this means that the charge and discharge of this first phase can be carried out through this surface and after hydrogen diffusion through this second phase. Hydrogen diffusion between the Laves phase and the secondary phase through metallurgical grain boundaries proceeds easily. Moreover, since the second phase can be hydrided, hydrogen diffusion through this phase is possible. These conclusions can be transposed to the two other alloy families, although to a lesser extent. The increase in reversible electrochemical capacity with nickel substitution is related to the decreasing stability of the hydrides. A really interesting capacity (330 mAh g^{-1}, 83% of the reversible hydrogen capacity) is obtained only for 0.6 alloys, the only ones with equilibrium pressure beyond 0.1 bar at room temperature. Moreover, the electrochemical activity of ZrNi and Zr_9Ni_{11} phases is perhaps less effective.

A similar phenomenon to that described here was observed by Gutjahr [6] in the discharge of alloys of the Ti–Ni system. In this system, the two phases TiNi and Ti_2Ni have low capacities due, for the first one, to small hydrogen absorption capacity and for the second one to the formation of a passivation layer. The coexistence of the two phases in a metallurgical composite leads to the charge and discharge of Ti_2Ni through the TiNi phase.

6. Conclusion

Study of the Zr–Ni–Cr phase diagram at 1000°C shows a large ternary extension of the stability ranges of the C14 and C15 phases as a function of nickel substitution. The determination of this isothermal section allows the synthesis of alloys where Laves phases of controlled composition are in equilibrium with a defined amount of secondary Zr–Ni phases. Nickel substitution in $ZrCr_2$ produces a large hydride destabilization that allows the thermodynamic properties of the hydride to be adapted to electrochemical application (reversible capacity superior to 3 H/f.u., plateau pressure in the range 0.1–1 bar). The hydrogenation properties of two-phase alloys are proportionally related to the quantity of each phase. However, we observe in the electrochemical reaction a considerable enhancement of the discharge capacities as compared with the capacities of each phase taken independently. The low capacity of the Laves phases is not caused by inadequate thermodynamic properties, but by poor surface transfer. Zr–Ni binaries have appropriate electrochemical activities but their low capacities are explained by the thermodynamic properties of their hydrides. With mixed phase alloys, we take the advantages of each phase (bulk properties of Laves phases and surface properties of Zr–Ni phases) and can finally obtain the charge and discharge of the Laves phase by passing through the secondary phase.

References

[1] M. Boulghallat, N. Gérard, O. Canet and A. Percheron-Guégan, *Z. Phys. Chem., 179* (1993) 211.
[2] S. Fujitani, I. Yonezu, T. Saito, N. Furukawa, E. Akiba, H. Hayakawa and S. Ono, *J. Less-Common Met., 172–174* (1991) 220.
[3] A. Züttel, F. Meli and L. Schlapbach, *J. Alloys Comp., 209* (1994) 99.
[4] P.H.L. Notten and P. Hokkeling, *J. Electrochem. Soc., 138* (7) (1991) 1877.
[5] S.R. Ovshinsky, M.A. Fetcenko and J. Ross, *Science, 260* (1993) 176.
[6] M.A. Gutjahr, *Ph.D. Thesis*, Geneva University, 1974.
[7] J.-M. Joubert, M. Latroche, A. Percheron-Guégan and I. Ansara, *J. Phase Equilib., 16* (6) (1995) 485.
[8] J. Rodriguez-Carvajal, *Proc. XV Congr. Int. Union of Crystallography, Satellite Meet. on Powder Diffraction, Toulouse, 1990*, pp. 1–127.
[9] D. Arias and J.P. Abriata, *Bull. Alloy Phase Diagr., 7* (3) (1986) 237.
[10] P. Nash and C.S. Jayanth, *Bull. Alloy Phase Diagr., 5* (2) (1984) 144.
[11] J.-M. Joubert, M. Latroche and A. Percheron-Guégan, *Proc. Int. Symp. on Metal Hydrogen Systems, Fujiyoshida, 1994* (*J. Alloys Comp., 231* (1995) 494).
[12] J.-C. Achard, A. Percheron-Guégan, H. Diaz, F. Briaucourt and F. Demany, *Proc. 2nd Int. Congr. on Hydrogen in Metals, Paris, 1977*, 1E12.